Microelectronics Reliability 171 (2025) 115785

Contents lists available at ScienceDirect

Microelectronics Reliability

journal homepage: www.elsevier.com/locate/microrel

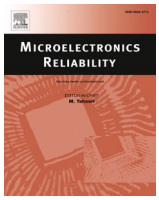

Research Paper

Performance characterization of lithium-ion battery and aging under constant stress conditions at low temperature☆

O. Rafik *, A. Capitaine, O. Briat, J.-M. Vinassa

Univ. Bordeaux, CNRS, Bordeaux INP, IMS, UMR 5218, F-33400 Talence, France

ARTICLE INFO

Keywords:
Lithium-ion battery
Cycling at low temperature
Lithium plating
Low-temperature performance
Iso-stress

ABSTRACT

This paper presents a comparison on cycling strategies conducted on an experimental study on an NMC lithium-ion battery. The investigation focused on examining the capacity degradation on batteries subjected to two cycling protocols, conducted at an ambient temperature of 0 °C and stress factors that depend on actual capacity instead of nominal capacity. The capacity losses were evaluated post-cycling, revealing a degradation of 28.63 % and 25.5 % for cells subjected to Protocol 1, whereas cells cycled under Protocol 2 exhibited lower capacity losses of 21.58 % and 20.73 %.This paper also presents the impact of the discharging current and the depth of discharge on capacity utilization to support the development of optimized cycling protocols for practical applications.

1. Introduction

The lifespan of the battery depends on the conditions of use. Hence an accelerated aging test is possible instead of a real use profile because it would take too much time. Accelerated aging serves as a cost-effective and efficient approach, providing cycling data in a short timeframe (days to months). This capability allows the prediction of the lifespan of Lithium-ion Batteries (LIBs) under diverse operational stresses. During accelerated aging tests, it is crucial to analyse the aging mechanisms of the battery, our objective is to focus on a specific degradation mechanism, as lithium plating, and to develop a dedicated accelerated aging tests to address it.

Lithium plating refers to the reduction of dissolved Li^+ ions in the electrolyte to form metallic lithium on the surface of the anode's active material. This reaction occurs instead of the usual intercalation of lithium into the lattice structure of the active material [1]. Lithium plating occurs when the negative electrode potential (NEP) drops below 0 V vs Li/Li^+. This phenomenon is influenced by several factors during charging: the NEP decreases with increasing state of charge (SOC), higher charging currents, and lower operating temperatures [2].

In lithium-ion batteries, the conversion between electrical energy and chemical energy is achieved through repeated lithium ions intercalation and deintercalation. Side chemical reactions can cause irreversible losses of electrolyte, active electrode materials, and lithium inventory; therefore, the capacity decreases over cycles [3].

Studies have shown that the build-up of solid electrolyte interphase (SEI) passive film layers and lithium-plating on the anode electrode occur due to the depletion of cyclable lithium ions [4,5]. The formation of a thick, uneven passive film on the material's surface decreases electrode porosity and blocks the flow of lithium ions, leading to increased resistance and reduced capacity over time [6]. The deposited lithium occupies the interstitial sites in the graphite lattice, the surface can become saturated [7], which reduce the active surface of the negative electrode and then increase the local current density. Therefore, any cycling procedure for lithium-ion batteries must consider these underlying limitations to ensure safe operation and an extended cycle life. Hence, subjecting the battery to a fixed stress factor relative to its nominal capacity may create the illusion of maintaining an iso-constraint. However, as the battery ages, it is crucial to recognize that in order to sustain an iso-constraint, the cycling must instead be adjusted according to a stress factor relative to the actual capacity, which decrease with aging.

For ease of use, the accelerated stress factors typically employed include ambient temperature (T), current rates (C-rate), state of charge (SOC), and depth of discharge (DOD). The C-rate is a normalized metric that specifies the constant-current charge or discharge rate of a cell in relation to its capacity, expressed as xC [8]. This value is calculated based on the nominal ampere-hour capacity Q_n, also known as the commercial capacity. For instance, a cell with a nominal capacity of $Q_n = 10$ Ah, when discharged at a rate of $10C_n$, would deliver energy at a

☆ This article is part of a Special issue entitled: 'ESREF 2024' published in Microelectronics Reliability.

* Corresponding author.
E-mail address: ossama.rafik@ims-bordeaux.fr (O. Rafik).

https://doi.org/10.1016/j.microrel.2025.115785
Received 22 November 2024; Received in revised form 13 March 2025; Accepted 10 May 2025
Available online 17 May 2025

current of $10*Q_n = 100$ A, completing a full discharge within approximately 0.1 h (6 min), assuming the cell's chemistry supports such a high discharge rate. Conversely, discharging at a $0.1C_n$ rate would correspond to a current of $0.1*Q_n = 1$ A, resulting in a discharge time of approximately 10 h. It is important to note that the relationship between C-rate and discharge duration is not perfectly linear; at $10C_n$, a cell may reach its minimum operational voltage before the expected 6 min, while at $0.1C_n$, the discharge time could exceed 10 h. This non-linear behaviour emphasizes the complexities of battery performance under different C-rates and the significant impact of electrochemical factors on discharge capacity. In this study, the C-rate C_n is referenced to the nominal capacity Q_n, whereas the C-rate C_a is based on the actual capacity Q_a. This differentiation is essential for accurately evaluating battery performance and examining how capacity degradation affects discharge behaviour.

Eddahech et al. [9] proposed an equivalent-circuit model for the impedance of the battery, in order to identify the main stress factors of aging, the authors considered the C-rate, SOC and the cell temperature as the main stress factors of aging in the case of power cycling. Vries et al [10] considered depths of discharge, with up to four series of charge discharge experiments. The authors found that the cycle life increases as the DOD is reduced or as the same amount of charge is extracted from a lower SOC. Maures et al. [11] developed a state of health (SoH) estimator utilizing data obtained from cycling cells under varying temperatures and charge/discharge rates (C-rates).

Despite the variety of publications detailing cycling lithium-ion batteries under diverse conditions, there is limited information available on how degradation processes evolve when discharge rates are linked to the actual capacity. In other words, most existing degradation models are only validated after cycling the battery under nominal discharge currents.

Nevertheless, up to now, there were very few interests, if any, in examining how the performance parameters of the battery are influenced by the operational conditions associated with the real state of the battery, rather than its nominal state. Therefore, in this study, we present a comparison of the battery performance and its reliance on the operational conditions at two distinct aging protocols. This comparison follows extensive aging tests, where the discharge current rate and depth of discharge depend on the actual capacity of the battery, instead of the nominal capacity.

2. Experimental

2.1. Lithium-ion cell characteristics

The cells evaluated in this study are identical to those previously analysed in [12]. These are lithium-ion NMC cells in a standardized 21,700 cylindrical format. Their key specifications are provided in Table 1.

2.2. Test procedure

The experimental tests were carried out using a Biologic BCS-815 electrochemical workstation, which features eight channels, each capable of managing charge and discharge currents of up to 15 A and Electrochemical Impedance Spectroscopy (EIS) measurements.

To cycle the cells under lithium plating conditions and to conduct reference performance tests (RPT), a climatic chamber was employed to maintain a temperature of 0 °C during cycling and 25 °C during RPT. To charge the cells, a constant current (CC) of $0.3C_n$ is applied to the cell until it reaches a maximum voltage of 4.2 V. Following this, a constant voltage (CV) is maintained until the charge current drops to $0.02C_n$. This two-step charging process ensures that the cell is fully charged while preventing overvoltage. The RPT were conducted at the beginning of cycling, and subsequently repeated every 90 cycles to evaluate both capacity and internal resistance. Capacity measurements were performed at 25 °C using a complete discharge with a constant current of $0.2C_n$. Internal resistance (R_{dch}) was assessed through high-power pulse characterization (HPPC). Specifically, following the capacity measurement at 25 °C, the cell was charged to SOC 50 % and then subjected to a discharge pulse of $1C_n$ for a duration of 10 s. The internal discharge resistance was subsequently calculated using Ohm's law. Electrochemical Impedance Spectroscopy (EIS) measurements are conducted at the start and end of cycling tests at 25 °C and SOC 50 %, also during cycling at 0 °C and SOC 50 % every 30 cycles to monitor changes in internal resistances. These measurements involve potentiostatic measurement taken across a frequency range of 2 kHz to 100 mHz. The excitation voltage used is $V_{ac} = 10$ mV.

Table 1
Characteristics of the tested cells.

Maximum voltage V_{max}	4.2 V
Minimum voltage V_{min}	2.5 V
Max charge current (25 °C)	0.3C
Max discharge current (25 °C)	1.5C

2.3. Aging protocols

Four cells were cycled at 0 °C using two distinct protocols, with C#1 and C#2 cells assigned to P1, C#3 and C4 assigned to P2. Fig. 1 shows the evolution of the cycling current of C#1 and C#3, one current cycle begins with a 30-min rest period, followed by a CCCV charging phase,

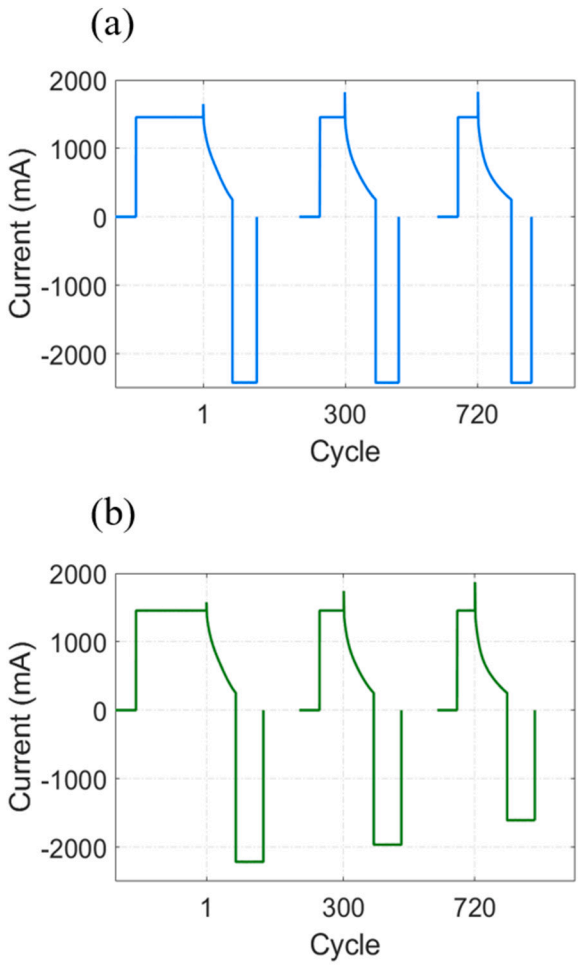

Fig. 1. The evolution of current for (a) cell#1 (b) cell#3. Cycled under P1 and P2 respectively.

and concludes with a constant-current discharge phase at I_{dch} until a specified discharge quantity Q_{dch} is reached. For P1, $I_{dch} = 0.5\ C_n$ and $Q_{dch} = 0.5\ Q_a$, with Q_{dch} adjusted every 30 cycles based on measurements of Q_a. P2 set $I_{dch} = 0.5\ C_a$ and $Q_{dch} = 0.5\ Q_a$, with both I_{dch} and Q_{dch} adjusted every 30 cycles after measuring Q_a. Actual capacity was evaluated in situ every 30 cycles at 0 °C using a full discharge at a constant current of $0.2C_n$. This systematic approach provides a detailed assessment of the effects of different cycling protocols on battery performance in low-temperature conditions.

3. Results and discussion

3.1. Evolution of the performance indicators

The energy and power performance of a battery are linked to its capacity (Q) and internal resistance (R), respectively. To study the evolution of these two quantities with aging, Q and R, are determined periodically at 25 °C ambient temperature. The evolution of these performance indicators is represented in Figs. 2 and 3, as a function of the discharge capacity throughput, which corresponds to the cumulated charge passing through the cell during the discharge. These results highlight a two-step performance degradation both on the capacity loss and on the resistance growth. Up to a discharged capacity throughput of 800 Ah, the degradation rate of the two indicators remains almost constant and equal for all cells. Then, this degradation rate increases significantly for cells cycled under P1 1, leading to a divergence on the evolution of both the capacity and the resistance with aging.

Cells cycled under P1 exhibited rapid degradation, retaining only 71.37 % and 74.50 % of their initial capacities for C#1 and C#2, respectively, at a discharged capacity throughput of approximately 1500 Ah. This degradation was accompanied by a significant increase in resistance, reaching 130.65 % and 141.50 % of the initial values. In contrast, cells subjected to P2 demonstrated a slower degradation rate, maintaining 78.42 % and 79.27 % of their initial capacities for C#3 and C#4, respectively, at a slightly higher throughput of approximately 1540 Ah. Furthermore, the resistance increase under P2 was comparatively lower, reaching 122 % and 120 %.

3.2. Electrochemical impedance spectroscopy

Fig. 4a presents the impedance spectrum at 0 °C and at SOC of 50 %, measured across a frequency range from 2 kHz to 100 mHz. The spectrum can be divided into three distinct regions [13]: the high-frequency region, the mid-frequency region, and the low-frequency region. In the high-frequency region, up to frequency f_0, impedance is mainly due to ionic conduction within the electrolyte and electronic conduction through the current collectors. This region displays a distorted semicircle, characteristic of these processes. In the mid-frequency region, spanning from f_0 to the transition frequency $f_{transition}$, impedance is

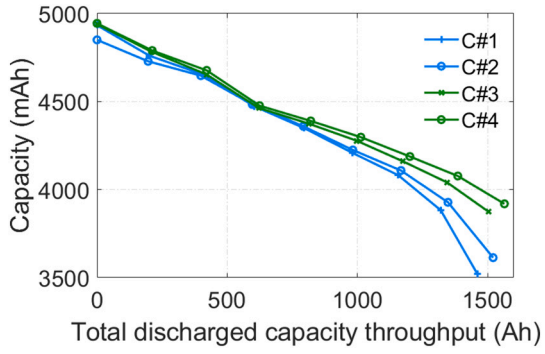

Fig. 2. Comparison of the capacity loss versus discharged Ah throughput, for the two cycling protocols.

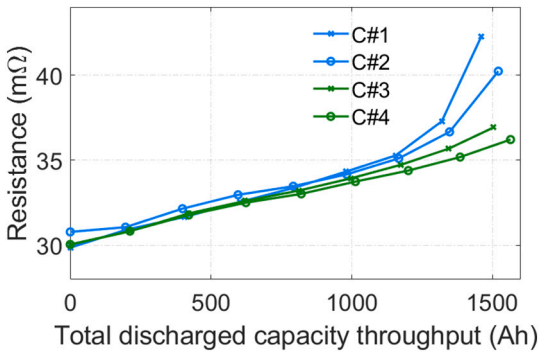

Fig. 3. Comparison of R_{dch} increase versus discharged.

associated with charge-transfer limitations at the electrode-electrolyte interfaces and ion migration through the solid electrolyte interphase (SEI) layer. Variations in the size of the mid-frequency semicircle, particularly in porous electrodes, indicate differences in interfacial properties, likely due to changes in SEI composition and structure. The low-frequency region, characterized by a 45° slope, reflects solid-state diffusion limitations within the electrodes.

Fig. 4b and c presents the impedance spectra at 0 °C and SOC 50 %, recorded every 30 cycles for Cell #1 and Cell #4, respectively. Over the course of aging, the impedance in the mid-frequency range exhibits a comparable rate of variation for both cycling protocols. Since charge transfer and ion migration through the solid electrolyte interphase (SEI) layer predominantly influence this frequency range, and given the well-established correlation between SEI thickness and aging, the observed mid-frequency impedance variations can be attributed to SEI evolution. Notably, as shown in Fig. 4b and c, Cell #4, cycled under protocol P2, demonstrates reduced SEI evolution compared to Cell #1.

Fig. 4d specifically depicts the ohmic component of the impedance, where the real part R_0 represents purely resistive behaviour, influenced by electrolyte conductivity and metal conductor resistances. R_0 is calculated by interpolating between the frequency points above and below the Re-axis. Degradation of the electrolyte affects ionic conduction, leading to an increase in R_0, whereas degradation of the current collectors is typically negligible. Both protocols exhibit a similar rate of R_0 increase until a discharged capacity of 500 Ah, where a slight degradation emerges for cells cycled under P1.

Fig. 5 displays impedance spectra at 25 °C and SOC 50 %, comparing the initial measurements with those taken after cycling under aging conditions. In contrast to the spectra at 0 °C, the effects of the cycling protocols on SEI contributions are more separated from other contributions at 25 °C. Cells cycled under P2, in particular, shows reduced SEI formation and, consequently, a smaller extent of degradation, indicating that P2 contributes to less SEI build-up and thereby mitigates overall degradation in comparison to the other protocol.

3.3. Resistance increase

As lithium-ion cells age, an increase in internal resistance is often observed due to the accumulation of side reaction products on the electrode particles, particularly at the electrolyte-electrode interfaces. This phenomenon, commonly driven by processes like the growth of the solid electrolyte interphase (SEI) layer and lithium plating, contributes to the gradual loss of active material and electrolyte over time. Consequently, under constant current conditions, this additional resistance generates a higher overpotential, causing the cell to reach its voltage cut-off more quickly when discharged, as illustrated in Fig. 6. This shortened voltage window per cycle reduces the usable capacity, energy, and power output with each successive cycle, highlighting the impact of internal resistance on cell performance and longevity. Moreover, as shown in Fig. 7, the energy delivered by the cell is further influenced by

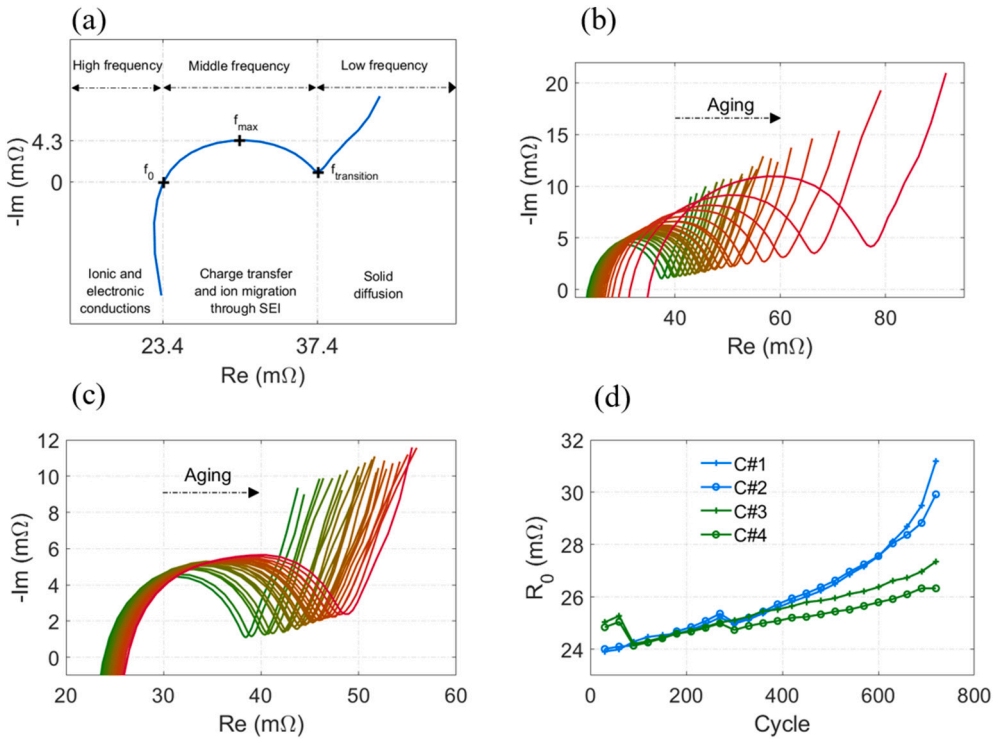

Fig. 4. Cell impedance at 0 °C: a) EIS plot at 50 % SOC, b) evolution of cell#1 impedance under P1, c) evolution of cell#4 impedance under P2, d) evolution of ohmic resistance.

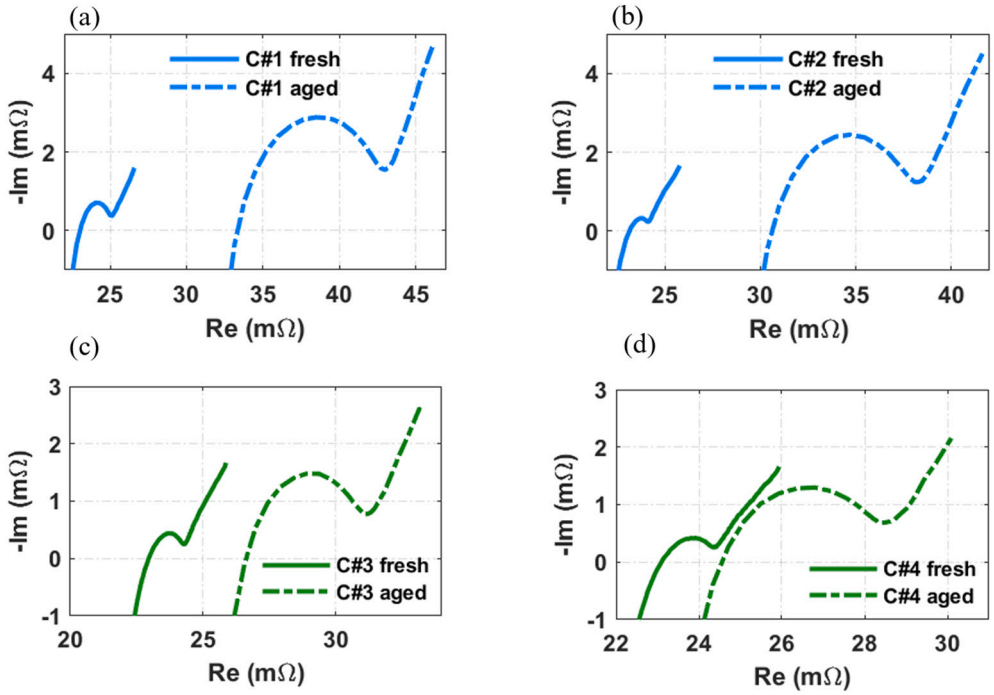

Fig. 5. EIS spectra of fresh and cycled cells (a), (b) under P1 and (c), (d) under P2 at 25 °C and SOC50%, ranging from 2 kHz to 100 mHz.

temperature increase. Temperature changes affect the reaction kinetics within the cell, which can either exacerbate or mitigate the effects of internal resistance on overpotential. Elevated temperatures, for instance, tend to reduce internal resistance temporarily due to increased ionic conductivity. However, repeated exposure to high temperatures can accelerate degradation mechanisms, thereby increasing resistance over the long term. The rate at which overpotential grows is determined by both the rate of resistance increase and the magnitude of the applied current. Higher discharge currents amplify the effects of internal resistance, accelerating the cell's approach to the cut-off voltage, especially at higher depths of discharge (DOD). As shown in Fig. 7 our comparison of protocol 1 and protocol 2, decreasing the discharge current and limiting the DOD led to a more stable temperature profile for cell#3 and cell#4, indicating a more favourable condition for prolonging cycle life.

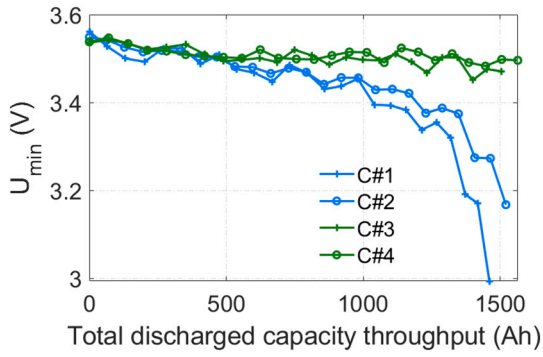

Fig. 6. Evolution of the discharge cut-off voltage vs total discharged capacity throughput.

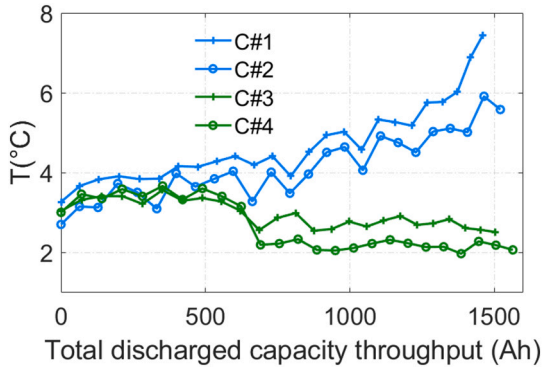

Fig. 7. Evolution of the cell temperature vs total discharged capacity throughput.

The reduction in current load minimizes heat generation, while the restricted DOD limits the extent of lithium plating and structural strain on the electrodes. In lithium-ion batteries, the voltage-capacity profiles exhibit relatively flat slopes at higher SOC or voltages, while lower SOCs and voltages correspond to steeper slopes. This difference in slope directly affects the cell's sensitivity to resistance changes: at high SOCs, the flat slope allows for smaller voltage changes in response to resistance increases, making the charge capacity highly sensitive to even small resistance growth. In contrast, at lower SOCs with steeper slopes, the discharge capacity initially remains relatively stable despite moderate resistance increases. However, once the cell reaches the inflection point on the voltage-capacity curve, the discharge capacity becomes increasingly sensitive to additional resistance and overpotential. This sensitivity leads to a sharp decline in deliverable capacity, energy, and power, as overpotential quickly drives the voltage to the cut-off limit. In summary, the interplay between internal resistance, applied current, and SOC significantly influences the aging behaviour and capacity fade of lithium-ion batteries. Managing discharge current and DOD is essential in reducing temperature growth and mitigating resistance growth, which in turn extends battery life. Understanding these complex interactions provides a foundation for optimizing battery management strategies, thereby improving the reliability and efficiency of lithium-ion batteries in practical applications.

4. Conclusion

This investigation into the cycling protocols of lithium-ion batteries reveals the substantial impact of discharge conditions on battery degradation and aging patterns. Protocol 2, which maintains a constant DOD and C-rate adapted to the actual capacity, demonstrated a slower degradation rate and less capacity decay compared to Protocol 1. Specifically, the study found that adjustments of discharge current and DOD contribute significantly to delaying the increase in internal resistance and capacity fade. These factors are crucial in minimizing overpotential effects, as evidenced by the greater stability in capacity and energy output under Protocol 2. Additionally, adaptation of the stress factor to the actual capacity plays a critical role in mitigating degradation and controlling temperature rise, thereby enhancing system stability and longevity during the aging process. This work supports the development of optimized cycling protocols that prioritize discharge current and DOD adjustments according to the actual capacity, in order to extend battery life. These results provide a foundation for further research on adaptive battery management strategies aimed at sustaining high performance and longevity under various operational stresses.

5. Future works

Future research can further refine cycling strategies by incorporating adaptive algorithms that dynamically adjust discharge currents and depth of discharge based on real-time battery health monitoring. Furthermore, testing these optimized cycling protocols in practical applications such as grid storage can validate their effectiveness in improving battery longevity under real-world operating conditions. By exploring how similar cycling protocols affect other lithium-ion chemistries, such as LFP (Lithium Iron Phosphate) or NCA (Nickel Cobalt Aluminum), would broaden the applicability of the findings.

CRediT authorship contribution statement

Rafik Ossama: Writing - Original draft, Writing - Review & editing, Data curation, Investigation.
Capitaine Armande: Writing - Original draft, Writing - Review & editing.
Briat Olivier: Writing - Original draft, Writing - Review & editing, Supervision.
Vinassa Jean-Michel: Writing - Original draft, Writing - Review & editing, Supervision.

Declaration of competing interest

The authors declare that they have no known competing financial interests or personal relationships that could have appeared to influence the work reported in this paper.

Data availability

The authors do not have permission to share data.

References

[1] V. Zinth, et al., Lithium plating in lithium-ion batteries at sub-ambient temperatures investigated by in situ neutron diffraction, J. Power Sources 271 (2014) 152–159, https://doi.org/10.1016/j.jpowsour.2014.07.168.
[2] T. Waldmann, B.I. Hogg, M. Wohlfahrt-Mehrens, Li Plating as Unwanted Side Reaction in Commercial Li-ion Cells – A Review, Elsevier B.V., Apr. 30, 2018, https://doi.org/10.1016/j.jpowsour.2018.02.063.
[3] X. Hu, L. Xu, X. Lin, M. Pecht, Battery lifetime prognostics, Joule 4 (2) (2020) 310–346, https://doi.org/10.1016/j.joule.2019.11.018 (Cell Press).
[4] W. Huang, et al., Evolution of the solid-electrolyte interphase on carbonaceous anodes visualized by atomic-resolution cryogenic electron microscopy, Nano Lett. 19 (8) (Aug. 2019) 5140–5148, https://doi.org/10.1021/acs.nanolett.9b01515.
[5] M.B. Pinson, M.Z. Bazant, Theory of SEI formation in rechargeable batteries: capacity fade, accelerated aging and lifetime prediction, J. Electrochem. Soc. 160 (2) (2013) A243–A250, https://doi.org/10.1149/2.044302jes.
[6] X.G. Yang, Y. Leng, G. Zhang, S. Ge, C.Y. Wang, Modeling of lithium plating induced aging of lithium-ion batteries: transition from linear to nonlinear aging, J. Power Sources 360 (2017) 28–40, https://doi.org/10.1016/j.jpowsour.2017.05.110.
[7] T. Gao, et al., Interplay of Lithium intercalation and plating on a single graphite particle, Joule 5 (2) (Feb. 2021) 393–414, https://doi.org/10.1016/j.joule.2020.12.020.
[8] Gregory Plett, Battery Management Systems, Volume I: Battery Modeling vol. 1, Artech, 2015.

[9] A. Eddahech, O. Briat, H. Henry, J.Y. Delétage, E. Woirgard, J.M. Vinassa, Ageing monitoring of lithium-ion cell during power cycling tests, Microelectron. Reliab. 51 (9–11) (2011) 1968–1971, https://doi.org/10.1016/j.microrel.2011.07.013.

[10] H. De Vries, T.T. Nguyen, B. Op Het Veld, Increasing the cycle life of lithium ion cells by partial state of charge cycling, Microelectron. Reliab. 55 (11) (2015) 2247–2253, https://doi.org/10.1016/j.microrel.2015.08.014.

[11] M. Maures, A. Capitaine, J.Y. Delétage, J.M. Vinassa, O. Briat, Lithium-ion battery SoH estimation based on incremental capacity peak tracking at several current levels for online application, Microelectron. Reliab. 114 (Nov. 2020), https://doi.org/10.1016/j.microrel.2020.113798.

[12] M. Lecompte, Julien Bernard, Elisa Calas, Lucas Richardet, Aurelien Guignard, François Duclaud, Damien Voyer, Maxime Montaru, Bruno Crouzevialle, Loic Lonardoni, Catherine Arnal, Olivier Briat, Armande Capitaine, Jean-Michel Vinassa, Eduardo Redondo-Iglesias, Serge Pelissier, Christophe Forgez, Guy Friedrich, Laurent Torcheux, Guillaume Bretin, Abdelhadi Asseban, Franck Sellier, An Li, Cedric De Vaulx, Kamel Azzouz, Jeremy Guazzagaloppa, Loic De Francqueville, Experimental assessment of high-energy high nickel-content NMC lithium-ion battery cycle life at cold temperatures, J. Energy Storage 94 (Jul. 2024) (2024) 112443, https://doi.org/10.1016/j.est.2024.112443.

[13] J. Ross Macdonald, William B. Johnson, Fundamentals of Impedance Spectroscopy Third edition, vol. chapter 1, John Wiley & Sons, Inc, 2018.